VALIDATION OF WAVE TRANSFORMATION MODELS FOR TROPICAL COASTAL ENVIRONMENTS

A THESIS SUBMITTED TO THE GRADUATE DIVISION
OF THE UNIVERSITY OF HAWAI'I IN PARTIAL FULFILLMENT
OF THE REQUIREMENTS FOR THE DEGREE OF

MASTER OF SCIENCE

IN

OCEAN AND RESOURCES ENGINEERING

DECEMBER 2007

By

Justin Avery Goo

Thesis Committee:

Kwok Fai Cheung, Chair
Mark Merrifield
Geno Pawlak

We certify that we have read this thesis and that, in our opinion, it is satisfactory in scope and quality as a thesis for the degree of Master of Science in Ocean and Resources Engineering.

THESIS COMMITTEE

Chairperson

ACKNOWLEDGEMENTS

I would like to thank my advisor Dr. Kwok Fai Cheung for his help and guidance through the course of this work. I would also like to thank Dr. Mark Merrifield and Dr. Geno Pawlak for providing the field data necessary to undertake this study as well as their useful comments and suggestions.

I would like to greatly thank the Ocean and Resources Engineering students who have worked with me through the course of the U.S. Army Corps of Engineers PILOT Project. In particular, I am appreciative to Dr. Yong Wei for providing the site figures and for leading me through the beginning phases of the project, Yongyan Wu for providing the COULWAVE data used in the project, Pablo Duarte Quiroga for providing the SWAN data and immeasurable help and input on the countless details involved with this project, and Volker Roeber for helping to generate the bathymetry at the study sites.

I would also like to thank Oliver Vetter for providing and explaining to me the field measurements taken at Ipan and Mokuleia. Lastly I would like to thank Ms. Edith Katada for all the help with all the departmental procedures and in processing all the necessary paperwork during my time in the Ocean and Resources Engineering Department.

Financial support in the form of a graduate research assistantship was provided by Healy Tibbitt Builders, Inc., U.S. Army Corps of Engineers, and Hawaii State Civil Defense.

ABSTRACT

Very few studies have been performed to validate near-shore wave models for fringing reef conditions. Fringing reefs dissipate large amounts of energy suddenly through plunging wave breakers, providing a direct contrast to the slower and gentler energy dissipation through spilling mechanisms that most coastal wave models are based upon. This study examines the application of the spectral wave models, Steady-State Spectral Wave Model (STWAVE) and Simulating Waves Nearshore (SWAN) as well as the Boussinesq model COULWAVE to describe wave transformation for the fringing reef conditions of Mokuleia, Oahu and Ipan, Guam as well as Waimea Bay, Oahu during swell events. STWAVE and SWAN describe the transformation in time of recorded wave spectra from the offshore buoy to the shore. COULWAVE provides a more precise, wave-by-wave description of the transformation along the nearshore instrument transects during low and high wave conditions. The results are compared to nearshore measurements recorded at the three sites. The spectral models STWAVE and SWAN give very similar results and compare reasonably well with measurements prior to wave breaking. Inside the surf zone, the differences between STWAVE, SWAN, and COULWAVE are noticeable and none of the models can consistently describe the surf zone wave height at all three sites. This is due to the differences in the predefined breaking criteria in the models as well as the frictional dissipation mechanisms employed. There appears to be a dependence upon the relative roles of wave breaking and bottom friction that may influence the general predictive capabilities of the models.

TABLE OF CONTENTS

LIST OF TABLES

LIST OF FIGURES

Chapter 1
Introduction

The tropical islands in the Pacific Ocean are typically fronted by fringing reefs and are open to large sea swells from distant pacific storms and waves from hurricanes. Field studies of wave transformation over fringing reefs have been performed (e.g. Black., 1978; Gerritsen., 1981; Lugo-Fernandez et al., 1998; Roberts et al., 1975; and Young, 1989). However, validating nearshore wave models under these conditions are less immediately evident. Fringing reefs have sharp transitions from deep to shallow water and a significant amount of wave energy is dissipated rapidly in the breaking process. This would contrast with the gentle energy dissipation assumptions that current nearshore wave models are based upon.

The Steady-State Spectral Wave Model (STWAVE) and Simulating Waves Nearshore (SWAN) are commonly used to simulate wave propagation and transformation from deep to shallow water. STWAVE is a steady-state finite difference model based upon the wave-action balance equation (Resio, 1987, 1988). SWAN can describe variation of sea state as a function of time through an implicit integration scheme and includes wave setup in the surf zone and more sophisticated nonlinear effects such as triad and quadric wave-wave interactions (Booji et al., 1999; and Ris et al., 1999). Recent advances in Boussinesq models allow for fully nonlinear and weakly dispersive long and intermediate waves over variable bathymetry with provisions for wetting and drying of the coastal land. In particular, Lynett et al. (2002) described a Boussinesq model known as COULWAVE, which has a robust algorithm to keep track of the moving waterline for inundation calculation. The formulation is based on Nwogu's (1993) approach, which provides the optimum agreement of the governing equations with the linear dispersion relation. Wave breaking is approximated by wave-steepness dependent diffusive terms in the momentum equation. In contrast to the spectral wave models, the Boussinesq models provide a wave-by-wave description of the processes in the surf and swash zones.

STWAVE, SWAN, and COULWAVE represent a wide range of coastal wave models. These models have been verified and validated with laboratory and field data, but have not been thoroughly examined for fringing reef conditions in tropical coastal environments. The present study, in conjunction with the Pacific Islands Land-Ocean Typhoon Experiment (PILOT), sponsored by the US Army Corps of Engineers, examines the implementation of these models to tropical coastal regions and evaluates their performance against field measurements from Mokuleia and Waimea Bay, Oahu and Ipan, Guam. The Mokuleia and Ipan sites are fronted by fringing reefs, where wave breaking occurs. The steep nearshore bathymetry and the lack of a reef system at Waimea Bay cause the waves to break directly in front of the beach. The selected sites provide different configurations and breaking wave conditions to test and identify the strengths and weaknesses of the models in describing wave breaking and transformation at tropical coasts. Improvements will be recommended to adapt these models predictive characteristics in fringing reef environments.

Chapter 2
Coastal Wave Models

STWAVE and SWAN are spectral models for coastal wave transformation, while COULWAVE is a phase-resolving model that provides wave-by-wave descriptions of the surf and swash zone processes. All three are depth-integrated wave models formulated in the Cartesian (x, y) horizontal plane. This section provides a brief description of the formulations of the three models and highlights their similarities and differences.

2.1 Spectral Wave Models

STWAVE 5.0 is a steady-state model for wave propagation and transformation from deep to shallow water (Resio, 1987, 1988). The physical problem is formulated on a half plane and the solution encompasses only the waves approaching the shoreline. The steady-state conservation of spectral action balance gives

$$(C_g)_x \frac{\partial}{\partial x} \frac{cc_g \cos(\mu-\theta)E(f,\theta)}{\omega} + (C_g)_y \frac{\partial}{\partial y} \frac{cc_g \cos(\mu-\theta)E(f,\theta)}{\omega} = \frac{S}{\omega} \qquad (1)$$

where $E(f, \theta)$ is the energy spectrum with f and θ indicating frequency and direction, μ is the wave ray direction, c represents the wave celerity and c_g the group velocity relative to an absolute reference frame, ω is the angular frequency relative to the current, and S represents second-order wind-wave growth, wave-wave interaction, and dissipation. The model includes refraction, shoaling, simplified diffraction, wave-current interaction as well as depth and steepness-limited wave breaking. With an input wave spectrum at the seaward boundary, a forward marching scheme with a finite difference technique tracks the nearshore transformation of spectral wave characteristics along predetermined wave rays. The wave rays are traced backward from the shoreline for each frequency-direction bin through Snell's law.

SWAN 40.51 is a third-generation spectral wave model that describes the evolution of a wave field from deep to shallow water under specified conditions of winds, currents, and bathymetry (Booij et al., 1999; and Ris et al., 1999). SWAN also uses an action balance equation, but implements an action spectrum $N(f, \theta)$ rather than an energy spectrum $E(f, \theta)$, since in the presence of currents, action density is conserved whereas energy density is not. The action balance is defined by

$$\frac{\partial N}{\partial t}+\frac{\partial}{\partial x}c_x N+\frac{\partial}{\partial y}c_y N+\frac{\partial}{\partial \omega}c_\sigma N+\frac{\partial}{\partial \theta}c_\theta N=\frac{S}{\omega} \tag{2}$$

where t denotes time, c_x and c_y are celerity components in the respective directions, and S represents wind input, triad and quadruplet wave-wave interactions, white capping, bottom friction as well as depth-induced wave breaking. The integration of the action balance equation is implemented with an implicit finite difference scheme with a constant time step. SWAN estimates the wave setup due to the radiation stress in the wave field. This is particularly important in shallow reef environments, where the magnitude of wave setup can affect the water depth, the breaking conditions, and subsequently the wave height.

The two spectral models employ different mechanisms for energy dissipation due to bottom friction and wave breaking. STWAVE uses either an input Manning coefficient, n, to account for the effects of bed roughness, or an empirically based JONSWAP friction coefficient, c_f, derived from the JONSWAP experiment that determines the frictional energy dissipation by sea swells over sand beds in the North Sea (Hasselman et al., 1973). The friction coefficient c_f is defined as Γ/g, where the recommended value of Γ is 0.038 m^2/s^3 for swell conditions and 0.067 m^2/s^3 for sea conditions. SWAN uses the eddy-viscosity model of Madsen et al. (1988) to account for the dissipation of an oscillatory flow due to bed roughness. The Madsen coefficient, K_N, uses the bottom roughness length scale to determine a non-dimensional friction factor,

f_{wr}, for frictional dissipation. SWAN also has a JONSWAP frictional coefficient, c_{JON}, which is equivalent to Γ in STWAVE with the same recommended values.

In the surf zone, STWAVE uses a strict depth and steepness limited breaking criterion, in which the maximum zero-moment wave height in the surf zone is defined by

$$H_{mo_{max}} = 0.1L \tanh kh \tag{3}$$

where L is the wavelength and h is the water depth. STWAVE reduces the spectral energy proportionally based on the difference between the calculated and maximum zero moment wave height. SWAN, on the other hand, adopts a depth-induced bore approach that fractionally reduces wave energy based on the Rayleigh distribution as the waves propagate towards shore. The energy dissipation per unit horizontal area due to wave breaking is defined by

$$D_{tot} = -\frac{1}{4}\alpha_{BJ} Q_b \left[\frac{\bar{\sigma}}{2\pi}\right] H_m^{\ 2} \tag{4}$$

where α_{BJ} is a free parameter with a default value of one, Q_b is the fraction of breaking waves in the Rayleigh distribution, $\bar{\sigma}$ is the mean frequency, and H_m is the maximum individual wave height that can exist at a given depth. The value of H_m is defined by

$$H_m = \gamma d \tag{5}$$

where d is the water depth including tides and wave setup and γ is the depth induced breaking parameter. SWAN uses a default $\gamma = 0.73$, but γ can be changed as desired by the user.

Both models use rectangular computational domains. STWAVE applies the input energy spectrum at the offshore boundary and shoals and refracts the spectrum to provide input along the two lateral boundaries. The boundary condition for SWAN is more flexible as the input wave spectrum can be a function of time and space along part or all of its ocean boundaries as specified by the user.

2.2 Deterministic Wave Models

Lynett et al. (2002) described a Boussinesq-type model known as COULWAVE for the evolution of fully nonlinear and weakly dispersive waves in immediate to shallow water. Let η denote the free surface elevation. The governing equations are given as

$$\begin{aligned}&\eta_t+\nabla\cdot\left[(h+\varepsilon\eta)\mathbf{u}\right]-\mu^2\nabla\cdot\{(h+\varepsilon\eta)[\left[\frac{1}{6}\left(\varepsilon^2\eta^2-\varepsilon\eta h+h^2\right)-\frac{1}{2}z_\alpha^2\right]\nabla(\nabla\cdot\mathbf{u})\\&+\left[\frac{1}{2}(\varepsilon\eta-h)-z_\alpha\right]\nabla\left[\nabla\cdot(h\mathbf{u})\right]]\}=O\left(\mu^4\right)\end{aligned} \tag{6}$$

$$\begin{aligned}&\mathbf{u}_t+\varepsilon\mathbf{u}\cdot\nabla\mathbf{u}+\nabla\eta+\mu^2\left\{\frac{1}{2}z_\alpha^2\nabla(\nabla\cdot\mathbf{u}_t)+z_\alpha\nabla\left[\nabla\cdot(h\mathbf{u}_t)\right]\right\}\\&+\varepsilon\mu^2\left\{\left[\nabla\cdot(h\mathbf{u})\right]\nabla\left[\nabla\cdot(h\mathbf{u})\right]-\nabla\left[\zeta\left(\nabla\cdot(h\mathbf{u}_t)\right)\right]+(\mathbf{u}\cdot\nabla z_\alpha)\nabla\left[\nabla\cdot(h\mathbf{u})\right]\right\}\\&+\varepsilon\mu^2\left\{z_\alpha\nabla\left[\mathbf{u}\cdot\nabla\left(\nabla\cdot(h\mathbf{u})\right)\right]+z_\alpha(\mathbf{u}\cdot\nabla z_\alpha)\nabla(\nabla\cdot\mathbf{u})+\frac{z_\alpha^2}{2}\nabla\left[\mathbf{u}\cdot\nabla(\nabla\cdot\mathbf{u})\right]\right\}\\&+\varepsilon^2\mu^2\nabla\left\{-\frac{\eta^2}{2}\nabla\cdot\mathbf{u}_t-\eta\mathbf{u}\cdot\nabla\left[\nabla\cdot(h\mathbf{u})\right]+\eta\left[\nabla\cdot(h\mathbf{u})\right]\nabla\cdot\mathbf{u}\right\}\\&+\varepsilon^3\mu^2\nabla\left\{\frac{\eta^2}{2}\left[(\nabla\cdot\mathbf{u})^2-\mathbf{u}\cdot\nabla(\nabla\cdot\mathbf{u})\right]\right\}+\mathbf{R}_f-\mathbf{R}_b=O\left(\mu^4\right)\end{aligned} \tag{7}$$

where ε and μ, account for the nonlinearity and frequency dispersion, and $\mathbf{R}_f$ and $\mathbf{R}_b$ account for bottom friction and wave breaking, and $\mathbf{u} = (u, v)$ is evaluated at $z_\alpha = -0.531h$ based on Nwogu (1993). The numerical model utilizes a fourth-order predictor-corrector scheme and tracks the moving waterline in the swash zone by extrapolating the solution onto the beach.

COULWAVE, similar to STWAVE, does not consider the oscillatory character of the flow in estimating energy dissipation due to bottom friction. The dissipation term is based on a Smagorinsky-type subgrid model to account for the effect of the resultant eddy viscosity on the underlying flow (Chen et al., 1999). The bottom friction is modeled by the quadratic law

$$\mathbf{R}_f = \frac{f}{d}\mathbf{u}|\mathbf{u}| \tag{8}$$

where f is a bottom friction coefficient and $d = h + \eta$ is the total water depth. Based on the approach of Chen et al. (2000) and Kennedy et al. (2000), energy dissipation due to wave breaking is approximated by

$$\mathbf{R}_b = \frac{1}{d}\left\{[\nu(du)_x]_x + \frac{1}{2}[\nu(du)_y + \nu(dv)_x]_y, [\nu(du)_y]_y + \frac{1}{2}[\nu(du)_y + \nu(dv)_x]_x\right\} \tag{9}$$

where ν is the eddy viscosity depending on the free surface elevation, water depth, and a mixing length coefficient (Zelt, 1991). For all breaking events, the eddy viscosity is filtered for stability using a three point filter before implementing in Eq. (9).

The computational domain is analogous to a rectangular laboratory wave basin with the modeled shoreline located at one end and dissipative sponge layers placed along the other three walls. Along a pre-defined line within the computational domain, waves are generated using a source function approach. The free surface elevation along the line source is given by

$$\eta(x, y, t) = \sum_{i=1}^{M_\omega}\sum_{j=1}^{M_\theta} a_{ij} \sin[k_i(x\cos\theta_j + y\sin\theta_j) - \omega_i t + \phi_{ij}] \tag{10}$$

where a_{ij} is the input discrete spectrum from SWAN, k_i is the wave number, ϕ_{ij} is a random phase shift, and M_ω and M_θ denotes the numbers of frequencies and directions bins respectively. The internal source generates the target waves through addition and subtraction of mass along the line source, emulating the excitation of a directional wave maker. Waves radiate out from the line source in both directions. Those propagate toward the shoreline are considered; dissipative sponge layers numerically absorb those propagate in other directions.

Chapter 3
Site Description and Model Setup

STWAVE, SWAN, and COULWAVE are used to describe wave transformation across the fringing reefs of Ipan, Guam and Mokuleia, Oahu. Fringing reefs are a particular type of coral reef, which exists in shallow waters near tropical islands and continents (Young, 1989). Fringing reefs are attached to land and have a typical profile characterized in Figure 1. The profile has a sharp transition from relatively deep to shallow water over a flat reef top (Hardy and Young, 1996). The calculation is also performed for Waimea, Oahu, where the steep nearshore bathymetry without a reef system provides different breaking wave conditions for the testing of the wave models.

3.1 Oahu, Hawaii

Oahu is one of the Hawaiian Islands in the Central North Pacific. Figure 2 shows the bathymetry around Oahu and the nested computational domains at the Waimea and Mokuleia sites. The bathymetry from coastline down to about 30 m water depth is obtained from the Scanning Hydrographic Operational Airborne LIDAR Survey (SHOALS) conducted by the US Army Corps of Engineers (USACE) at 3-m resolution and for deeper waters data is obtained from United States Geological Survey (USGS) at 5-s (~150-m) resolution. Mokuleia and Waimea, which are located on Oahu's North Shore, are subject to large northwest swells originating from storms in the North Pacific typically during October to March. The nearshore waters are relatively calm during the other months. The Scripps Institute of Oceanography Coastal Data Information Program (CDIP) Directional Waverider Buoy 106/206 is located offshore of the two sites at approximately 200 m water depth and provides input conditions for the model study.

Figure 3 displays the nested computational domains at Waimea for the spectral and Boussinesq model as well as the locations of wave measurements. Waimea Bay is approximately 640 m × 290 m with depth up to 10 m near the mouth. The slope approaching the mouth is fairly steep. The lack of a reef system fronting the shoreline causes the waves to break directly in front of the beach. The computational domain for spectral models encompass all of Figure 3, covering a 13,000 m × 16,000 m area surrounding Waimea that extends beyond the 200-m contour, where Buoy 206 is located. The models use a uniform 50-m resolution resulting in a 261 × 321 grid. The computational domain for the Boussinesq model is shown in the smaller shaded area within Figure 3. The 2,500 m by 2,300 m domain has a 4-m resolution resulting in a 625 × 575 grid. For Mokuleia, the computational domain for the spectral models encompasses all of Figure 4 with an 18,500 m × 13,500 m area from the shore to the 200-m contour, where Buoy 106 is located. The grid has a uniform 50-m resolution resulting in 371 × 291 grid. The Boussinesq model grid covers a 1,400 by 1,400 m area at 4 m resolution.

In the spectral wave models, the seabed beyond the 200-m contour is considered to have a uniform depth of 200 m. Directional wave spectra from Buoy 106/206 at 200 m of water provide the input wave conditions at the two sites. An Acoustic Doppler Current Profiler (ADCP) and two Aquadopp's (AQDP) at waters depths of 21 m, 11 m, and 7 m respectively, provide measured wave conditions for comparison with the model output at Waimea. These instruments were located along a cross-shore transect near the centerline of the bay. All three sensors recorded data at 1 Hz continuously during the deployment. Ideally the directional spectrum output from the ADCP would be used to provide the input wave conditions at the seaward boundary for the Boussinesq model but it was unavailable at the time. Thus the directional spectrum output of SWAN was used instead. In the computation, the region offshore of the 21-m contour, where the ADCP was located, is considered to have a uniform depth of 21 m for the development of the incident waves from the wavemaker.

For Mokuleia, Seabird Electronics (SBE) bottom pressure recorders were deployed at approximately 1, 5, and 10 m water depth as illustrated in Figure 4. Data was recorded continually during the deployment at 1Hz. Fringing reefs are present along the coastline. The profile along the instruments across the Boussinesq model domain shows a relatively plain slope (~1/65) leading to a relatively flat reef top that extends to the shoreline. Spectral data from SWAN at SBE59 located at 10 m water depth provides the input wave conditions at the seaward boundary of the Boussinesq model. Similarly, the region offshore of the 10-m contour is considered to have a uniform depth of 10 m for the development of the incident waves from the wavemaker.

3.2 Guam, Mariana Islands

Guam is one of the Mariana Islands in the western Pacific Ocean. Figure 5 shows a map of Guam overlaid with the bathymetry and topography at the central section of the island. The bathymetry for the nearshore region was obtained from SHOALS and deeper regions were obtained from a dataset compiled by the USACE. The figure also shows the nested computational domains at Ipan. This location is sheltered from swells generated in the North and South Pacific, but is exposed to wind waves approaching from the east and occasional storm waves from tropical cyclones. The Scripps Institute of Oceanography Coastal Data Information Program (CDIP) Directional Waverider Buoy 121 is located offshore of Ipan at approximately 200 m water depth.

The computational domain for the spectral models encompass all of Figure 6 with a 3,000 m × 6,000 m area surrounding Ipan and extends beyond the 200-m contour, where the offshore buoy is located. The model, which has a uniform 25-m resolution resulting in a 121 × 241 grid, is significantly smaller than those of Waimea and Mokuleia. A finer 25-m grid resolution is needed to better resolve the steep fringing reef off the Ipan coast. In the computation, the water depth beyond the 200-m contour is considered to have a uniform water depth of 200 m and the measured spectral wave conditions from Buoy 121 define the input conditions along the eastern boundary.

The computational domain for the Boussinesq model, which is shown by the smaller shaded grid within Figure 6, covers a 1,600 m by 2,300 m area with 5-m resolution resulting in a 320 × 460 grid. The region has a very steep reef face as evidenced by the cross-shore bathymetry transect. The reef top is very shallow (~0.5m) with some portions being above the mean lower low water (MLLW) level. One AQDP was deployed directly in front of the reef face and three AQDP were deployed over the reef top with water depth less than 1 m. The AQDP's sampled 1024 measurements every 1200 seconds at 1Hz. Data was recorded in 20 minute intervals with 10 minutes in between measurements.

Chapter 4
Results and Discussion

Table 1 summarizes the swell and sea events for the comparative study at Waimea, Mokuleia, and Ipan. The wind conditions, which may be included in the spectral models, are not considered because of the small fetch in the computational domains. The still-water level in the wave models is adjusted by tidal data obtained from the National Oceanic and Atmosphere Administration (NOAA) Tides and Currents Historic Data Measurements. This is particularly important for the Mokuleia and Ipan sites, where the water depth over the shallow reef depends largely on the tidal level. The significant wave height and peak period are calculated by a Fast Fourier Transform algorithm that generates an energy spectrum from a 20-minute long time series of surface elevation or pressure recordings at 1Hz. Surface elevation data was provided for Mokuleia, while pressure recordings were provided for Ipan and Waimea. To test the general predictive capabilities of the models, all encompassing frictional dissipation coefficients were used in the initial study, with more site specific values applied as necessary. The modeling of the volcanic seafloor and rough reef surfaces were estimated by the models. STWAVE uses an $n = 0.035$, SWAN used $K_N = 0.2$ m, and COULWAVE uses a friction coefficient of 0.01, which corresponds to a Manning coefficient of 0.035 at a typical water depth of 2 m over the reef top. Field observations at Ipan and Mokuleia reference to the field measurement portion of the PILOT project (Vetter, 2006) and observations at Waimea reference the original study of the acquired dataset (Mortensen, 2006).

4.1 Waimea, Oahu

Field measurements were taken from the last swell event of the season from 19:00 UTC March 19, 2006 to 17:00 UTC March 21, 2006. Buoy 206 recorded an average significant wave height of 2.20 m and an average peak period of 14.8 s during the 46-hour event.

The waves enter the spectral model domain from the north. Figure 7 compares the computed significant wave height and peak period with offshore and nearshore measurements during the event. The buoy data indicates that the initial event includes of a mix of swell and local wind waves resulting in alternation of the peak period between 6 and 18 s. The swell built up over time and peaked near 15:30 UTC March 20 with a significant wave height of 2.85 m and a peak period of 13.3 s. The swell maintained a significant wave height of at least 2.5 m for about 12 hours, while the peak period shows a steady decline from 18.2 s to 13.3 s during the event.

The buoy measurements provide the input wave conditions at the boundaries that should reach Buoy 206 inside the domain without transformation. STWAVE shows near-perfect agreement with the measured data at the buoy as expected. SWAN, however, shows noticeable underestimation of the significant wave heights. This is due to the positioning of the buoy near the north-south lateral boundary, where only the westerly components of the input wave spectrum can enter the computational domain. This results in underestimation of the significant wave height near the west boundary, but should have minimal effects to the study site, which is located in the eastern half of the domain. An output point for SWAN was put in the middle of the domain 500 m away from the offshore boundary and showed very good agreement with the buoy data. STWAVE, on the other hand, has an open boundary condition which reflects interior grid points across the boundary to help limit effects of the lateral boundary.

The northerly incident waves refract towards the coastline and show an average 35% reduction of the significant wave height at the ADCP in 21 m of water. The effects of refraction are significant as the spectral models show on average a 45° change in mean wave direction from Buoy 206 to the ADCP. Both spectral models potentially overestimate the significant wave heights at the ADCP due to their inability to resolve the visually observed wave reflection from the southern entrance of the bay that forms partial standing waves in the opposite direction of swell propagation outside the bay. Initially the goal was to extract the reflected energy from the directional spectrum and provide a more direct comparison of wave heights, but this was not possible without a directional spectrum from the ADCP. The waves continue to refract into the bay as the wave heights are further reduced 35% at the bay entrance. The effects of refraction are again significant as the spectral models show a 20° change in mean wave direction from the ADCP to AQDP1. Both models continue to overestimate significant wave heights at AQDP1.

As the waves approach AQDP2, situated in the middle of the bay, the recorded data shows a 20% increase in wave height from the bay entrance. This appears likely due to shoaling; however, there is a possibility that the increase in significant wave height is due to AQDP2 being located at an anti-node of the standing waves in the longshore direction of the bay created from the reflection at the southern entrance. The standing wave pattern was observed by *Mortensen* [2005], but could not be confirmed in the field data as there were not enough sensors in the longshore direction to make an accurate assessment of this phenomenon. The two spectral models underestimate the measurements at AQDP2, as they show a slight 10% decrease in wave heights primarily through refraction and slightly due to friction instead of the increase shown by the field data. The magnitude of wave height reduction between AQDP1 and AQDP2 is nearly the same with friction turned both on and off by the models showing that the reduction in wave heights by the spectral models is primarily through refraction. However, the effects of refraction are less significant as there is a small 5° change in mean wave direction between AQDP1 and AQDP2 by the spectral models. The spectral models' inaccuracies are likely due to their inability in replicating the effects of reflection off the southern bay entrance. The computed results show a continuous decrease of the wave height from the ADCP to AQDP2 during the entire event. All the waves were observed to break shoreward of AQDP2 directly on the shoreline. The peak period remains quite steady across the shore during the initial swell, with a small influence from the wind waves. The sensors show minor cross-shore fluctuations of the dominant frequency component after the peak of the event.

Figure 8 provides a comparison of the results from the three models across the instrument transect at the peak of the swell as well as a smaller event for reference. A 25-m grid resolution was used in the cross shore comparison to better capture the bathymetric features. Using a 25-m resolution for the entire event would be too computationally time consuming and thus it was only used in the cross shore comparison. The longshore variability is shown in the figure with the thicker lines indicating the wave heights and bathymetry along the instrument transect and the thinner lines indicating the data at ±25 m from the instrument transect. Table 2 provides a summary of the wave conditions. During both events, the measured data shows a decrease of the significant wave height between ADCP and AQDP1 caused primarily through refraction as waves propagate into entrance of the bay. As the waves approach AQDP2, wave heights increase before breaking in front of the shoreline. The increase is likely due to shoaling and is possibly aided by longshore standing wave patterns that may exist within the bay. The input conditions for COULWAVE come from the SWAN output at the ADCP. The initial good agreement between the COULWAVE and SWAN significant wave heights shows proper implementation of the input conditions for COULWAVE. Both spectral models fail to capture the trend of the measured data. Wave heights decrease continually through refraction from the ADCP to AQDP2. There is a small increase in wave heights due to shoaling just prior to breaking near the shoreline. The only noticeable longshore variability in the data appears to be very close to the shoreline as location of the shoreline changes causing wave breaking to occur at different locations. COULWAVE reproduces the overall trends but cannot describe the sharp increase of the wave height over due to either shoaling over the steep nearshore slope or from the possible longshore standing wave patterns present within the bay.

4.2 Mokuleia, Oahu

The record chosen for Mokuleia contains two mixed events with seas and swells and one large swell event over a 13-day period. The two mixed events occur between March 28 and April 5 and are followed by the swell event from April 6 to April 9. Buoy 106 recorded an average significant wave height and peak period of 1.78 m and 12.6 s during the mixed events and 2.40 m and 13.4 s during the swell. Figure 9 compares the computed significant wave height and peak period with offshore and nearshore measurements during the three events. The buoy data shows the higher peak of the mixed events had a significant wave height of 2.90 m around 08:00 UTC April 3, 2004. The swell reached a peak significant wave height of 4.10 m around 08:00 UTC April 7, 2004. The buoy data shows a strong bimodal tendency with alternating peak periods throughout the two events.

The waves during the entire record approach from northwest. The spectral models show waves refract by approximately 15° from the offshore buoy to SBE59 (~10m). The measured data shows on average a 25% decrease in significant wave height through refraction and frictional dissipation over the rough reef. Between SBE59 and SBE55 (~5 m) the measured data shows on average a slight 7% drop in the wave height during the mixed events possibly due to the effects of shoaling being canceled out from the effects of refraction and friction of the rough reef. During the swell event, there is a sharper drop off in wave heights between SBE59 and SBE55 likely indicating wave breaking between the sensors. The majority of the remaining wave energy is dissipated through wave breaking and frictional dissipation over the rough reef surface between SBE55 and the shallowest sensor SBE57 (~1m), which shows almost no wave energy. The spikes in the wave period plot are due to infragravity energy being the dominant component in the energy spectrum. It is unclear exactly how the complete dissipation of wave energy is occurring in between the two sensors as measurements were not available in between, leaving the general surf zone being poorly defined.

The reef at Mokuleia is extremely rough with the observed roughness scale being up to ~0.5 m at some locations. In a previous study performed at a barrier reef in Kaneohe Bay, Oahu, Hawaii, the rate of energy dissipation through bottom friction within the surf zone was comparable to that of wave breaking during small to medium wave conditions and that during larger wave conditions breaking was the more influential component (Lowe et al., 2005). Due to the significant roughness of the reef at Mokuleia, it appears possible that dissipation through bottom friction could be significant and play as important a role as that of wave breaking, particularly during the mixed events.

Results from both spectral wave models show near-perfect agreement with the measured significant wave height and peak period at Buoy 106 confirming that the boundary condition has been properly applied. SWAN produces very good agreement with the significant wave heights recorded at SBE59 and SBE55 during the three events. STWAVE overestimates the wave heights at SBE55 and SBE59 during the mixed events and shows a smaller wave height reduction at SBE55 from wave breaking than SWAN during the swell. The difference in the two models during the mixed event is likely due to different formulations for frictional dissipation. At SBE57, the models determine the wave height based on their depth limited breaking schemes as the computed wave height becomes depth-limited and follows the tidal signal over the shallow reef. Both models overestimate the wave heights as they are unable to reduce wave energy through their wave breaking and frictional dissipation mechanisms to the extent that is occurring in the field. Based upon the initially assumed frictional values, it is difficult to tell whether the inability of the spectral models to match the energy dissipation between SBE55 and SBE57 is due to their breaking or frictional dissipation mechanisms.

Testing of the frictional parameters for both spectral models were performed to determine if a better match to the field data could be obtained by the spectral models. It was determined by Lowe et al. (2005) that the friction factor over the reef at Kaneohe Bay could be approximately thirty times greater than that of a sand bed. For STWAVE a c_f, thirty times ($c_f = 0.12$) over the recommended value for sand beds ($c_f = 0.04$) was used to determine if any improvements to the results could be obtained. Figure 10 shows that increasing the bottom friction helps in reducing wave energy at SBE57, but also results in STWAVE now underestimating the wave heights at SBE55 and SBE59. When increasing the c_{JON} to 1.14, 30 times the recommended sand bed value for SWAN, the same trend as STWAVE was apparent. In SWAN, K_N was varied between 0 and 1.0 to increase the roughness scale. The results in Figure 11 shows that increasing K_N helps to better reduce wave energy at SBE57, but again leads to an underestimation of wave heights at SBE55 and SBE59. It appears that the roughness has a greater effect shoreward of SBE59 in both models.

Figure 12 provides a comparison of the significant wave heights from the three models along the instrument transect at the peaks of the mixed and swell events as well as a calmer time during the observation period for comparison purposes. Table 3 summarizes the wave conditions during the three events. Again a 25-m resolution grid was used to better capture the bathymetric features. The thinner lines indicate the wave heights and bathymetry at ± 25 m from the instrument transect. It is apparent through initial visual inspection that there is little variability in the output data in the longshore direction. The significant wave heights along the instrument transect by STWAVE and SWAN during the calmer time shows good agreement initially but appear to be over-predicted when wave breaking occurs. In reality there is a significant reduction in wave height between SBE55 and SBE57 through wave breaking or friction as no swell energy is apparent at SBE57. The spectral models show a gradual decline of the wave height under the calm wave conditions. This is likely due to an underestimation of roughness with the initial frictional parameters as bottom friction should be as significant as wave breaking during smaller wave conditions. COULWAVE uses the SWAN output spectrum at the SBE59 as boundary conditions. The COULWAVE data shows a gradual and complete reduction in wave energy through wave breaking and friction.

The data at the peak of the mixed event shows the classic shoaling and breaking pattern of regular waves by STWAVE, while SWAN shows increasing dissipation of the wave energy toward the shore. The cause for the contrasting trends is due to their different breaking mechanisms. STWAVE uses a strict depth and steepness limited breaking scheme that shoals the significant wave height to a peak value before the breaking mechanism kicks in to dissipate the wave energy. SWAN, on the other hand, uses the Rayleigh distribution to fractionally reduce wave components that exceed the predefined steepness limit. This explains the initially gradual reduction of wave energy as only the largest waves in the tail end of the Rayleigh distribution breaks. As waves progress to shallower waters, a greater portion of the waves within the Rayleigh distribution break and the drop off in the significant wave heights becomes more dramatic. Both spectral models are unable to reproduce the total dissipation of wave energy through bottom friction and wave breaking. COULWAVE manages to reproduce the complete reduction in wave energy through breaking over the rough reef. The location of the breaker is likely off due to the breaking criteria in the model. COULWAVE produces better agreement with the measured wave height at SBE57 because of the large amount of energy it manages to dissipate over the reef.

During the peak of the swell event, STWAVE and SWAN show similar trends. Both spectral models show an initial slow reduction in wave heights from breaking that intensifies further along the reef face. COULWAVE again produces better agreement with the field data at the reef top as the wave energy has been completely reduced. In this case it appears breaking is sufficient in reducing the majority of wave energy and frictional dissipation is of less importance as this profile provides the best agreement at SBE57. This is along the lines of what was determined by Lowe et al. (2005), in which the importance of friction was less during larger wave conditions.

Testing of the frictional components along the cross-shore transect were also performed to determine the effects bottom friction on the computed wave height. SWAN was used over STWAVE as a friction coefficient f_{wr} can be determined from an input value of K_N related to existing roughness scales. STWAVE's coefficients have no dependence upon physical roughness scales and would need to be empirically fit to each site. Testing for COULWAVE was not performed as it is both computationally intensive and highly unstable. Small changes to the input conditions can cause the model to crash and thus sensitivity studies were not performed. However with its initially assumed frictional input, there is already a complete reduction wave height during all three profiles indicating that testing of the frictional parameters is unnecessary.

Figure 13 shows a comparison of the wave height distribution obtained with K_N = 0.2 and K_N = 1.0 in SWAN. With the initially assumed K_N = 0.2 m, f_{wr} varys with the peak period and gives rise to 0.08, 0.09, and 0.06 for the sequence of three events in Figure 13. The respective values of f_{wr} for a larger K_N of 1.0 are 0.26, 0.3, and 0.22, which are around the range of values found at Kaneohe Bay. The results with both K_N = 0.2 and 1.0 show the same trend. However, the use of K_N = 1.0 dissipates more energy near the coastline and gives better agreement with the measurements at SBE57, but underestimates wave heights at SBE55 offshore of the reef top. When viewing the cross-shore wave height with K_N = 0.2, it appears the field data could be properly matched if the breaking mechanism of SWAN reduced greater amounts of wave energy. It appears that better overall agreement cannot be obtained by just changing the friction coefficient.

At Mokuleia, frictional dissipation appears to play a significant part in wave height reduction during the shorter period mixed events. The general predictive capabilities of SWAN appear to be very good outside of the surf zone. STWAVE slightly overestimates wave heights and likely choosing a more appropriate Manning or JONSWAP coefficient will help improve the results. Both models are less accurate within the surf zone, particularly during the mixed events. To more precisely determine the current inaccuracies of the spectral models in the surf zone, it appears that more comprehensive field measurements are required as well as developing a better understanding of the general roughness scale of the reef as well as its spatial variability. This will help to better determine the wave height evolution along the cross-shore transect and help to give better insight into the relative roles of breaking and friction along the cross shore. If there is a sharp drop off in wave heights in the surf zone, the spectral models breaking mechanisms may be underestimating breaking energy dissipation and if a slower reduction in wave heights is present, than the underestimation of energy dissipation could be from underestimation of the actual roughness at Mokuleia. In any case, it appears that appropriate roughness scales must be determined for the best predictions and commonly used friction factors cannot accurately predict data in areas where the frictional effects of bed forms are significant. COULWAVE does a better job in matching the expected amount of energy dissipation during the peak event. It also appears to better replicate the data trend as input conditions become more energetic.

4.3 Ipan, Guam

The event chosen for Guam is primarily a wind wave event from October 16 to 24, 2005. Buoy 121 recorded an average significant wave height of 1.51 m and an average peak period of 11.0 s during the 9-day event. Figure 14 compares the computed and measured significant wave heights and peak periods at the buoy and sensors. The waves approached the site from east-northeast and reached a maximum significant wave height of 2.34 m at

Buoy 121 at 5:00 UTC October 20. As the waves approach SBE10 (~7.8m), located offshore off the reef face, the wave heights are reduced by approximately 30%. It appears that this is primarily due to frictional dissipation from offshore reef that was noted to be extremely rough. The effects of refraction are likely small as the spectral models show an average 3^{o} change in wave direction from Buoy 121 to SBE10. Wave heights increase slightly by 10% due to apparent shoaling between SBE10 and AQDP9 (~5.73m), which is situated at the edge of the reef face. Wave breaking is visually observed between AQDP09 and AQDP07 (~0.24m), situated approximately 10 m landward from the reef edge, resulting in a dramatic reduction of the significant wave heights at AQDP07. The majority of the wave energy is dissipated within 30 m of the reef edge, leaving almost no visible wave breaking bores at AQDP05 (~0.63m) and AQDP03 (~0.50m). The effects of bottom friction along the reef face and reef top are significantly smoother than offshore of the reef face. The roughness scale of the nearshore reef is ~0.1 m, approximately five times smoother than at Mokuleia. At Ipan wave breaking is assumed to dissipate the majority of the wave energy with frictional dissipation reducing any leftover energy along the reef top. The cause for the large spikes in the peak period plot in B03, B05, and B07 is due to dramatic reduction of the sea and swell energy bands leaving primarily infragravity band energy over the reef top.

The spectral model results show near-perfect agreement with the measured significant wave heights and peak periods at Buoy 121. Both models overestimate the significant wave height at SBE10 and AQDP09. The overestimation is likely caused by an underestimation of the roughness offshore reef by the initially assumed frictional coefficients. Increasing the roughness in SWAN to $K_N = 1.5$, 30 times larger than the default value of SWAN, provides little change in the wave heights at SBE10 and shows no major changes at the rest of the sensors. This indicates that the offshore reef could have significantly larger roughness features than what is assumed or energy is being dissipated through other measures. The reef leading up to the reef edge was noted to be very porous allowing wave energy to pass through and percolate up at the reef edge. This effect probably dissipates wave energy from but it was unclear how much of an effect this truly has. This phenomenon was not well understood but could be a reason for the overestimation by the spectral models as they would be incapable of capturing this complex process. The models show that most of significant energy is dissipated through wave breaking between AQDP09 and AQDP07. The gaps in the SWAN data at AQDP07 occur because the sensor is above the sea level at lower tides. The wave heights are further reduced through wave breaking and frictional dissipation as they reach AQDP05. The reduction of wave height from AQDP05 to AQDP03 is entirely due to frictional dissipation as both spectral models are no longer actively breaking waves. The computed wave height profiles at AQDP07, AQDP05, and AQDP03 mirror the tides at the site as a result of their depth-limited conditions. The higher wave heights computed by SWAN at AQDP07 sensors is likely due to its inclusion of wave setup that allows for higher water depths and higher computed wave heights. Upon reaching AQDP03 and AQDP05, almost all wave energy has been dissipated through wave breaking and friction and the models have better agreement between them.

Figure 15 shows the computed and measured significant wave heights along the cross-shore instrument transect during the peak of the event and during a calmer time of the record. COULWAVE data was not included for Ipan as the extremely shallow water depth over the reef top causes instabilities within the model. Table 4 summarizes the wave conditions. Again the thinner lines indicate the longshore variability of the data ±25 m from the instrument transect. The spur and groove morphology present at Ipan is apparent as the location of the reef edge is shifting along the shoreline. Though there is spatial variability in the wave height plots, the reduction in wave heights from breaking appear to occur directly on the reef edge at all locations. The spectral models reproduce the trend of the measurements in both cases that includes initial shoaling of the waves over the reef face followed by sharp drop offs of the wave height leading up the reef crest. The sudden transition from the steep reef face (~1/20) to the shallow reef top, forces STWAVE and SWAN to more quickly reduce wave heights as they break over the reef edge. Both models show a rapid reduction in wave heights through wave breaking. The extremely low water depth over the reef top forces the models to reduce wave heights to near zero levels over the reef top.

SWAN appears to better match the trend of the wave breaking along the cross-shore transect than STWAVE. SWAN shows a more gradual breaking trend that better match the wave height at AQDP07 within the surf zone. STWAVE on the other hand shows a sharper reduction in wave heights through wave breaking and underestimates wave heights at AQDP07. The reason for the contrasting trends could be the inclusion of wave setup in SWAN that allows a slightly larger water depth and subsequently the wave height at AQDP07. During the peak event, the maximum computed setup by SWAN was ~0.3 m and during the calmer event the maximum computed setup was ~0.15 m. The difference could also be due to the differences in their breaking mechanisms. The breaking mechanism of STWAVE directly reduces wave energy from the spectrum whenever the depth and steepness limit is exceeded. SWAN employs a fractional dissipation rate that should more slowly dissipate wave energy through breaking. At AQDP03 and AQDP05, situated shoreward of the surfzone, both models correctly show a near complete reduction in wave energy primarily through wave breaking over the reef face. The slight underestimation of wave heights would be expected as the spectral models are incapable of generating the infragravity motions that constitute the majority of the wave energy present at the AQDP03 and AQDP05.

The spectral models seem to be more capable of being used for predictive purposes at Ipan as opposed to Mokuleia. The better predictive capability at Ipan appears to be due to the dominance of wave breaking as well as the smaller water depth over the reef top that allows wave heights to be more sufficiently reduced through breaking. SWAN appears to be the better of the two as it does a very good job in replicating the wave height reduction through breaking as long as the reef is completely submerged. During lower tides when portions of the reef top are exposed, STWAVE is able to produce outputs, while SWAN is not.

Chapter 5
Conclusions and Recommendations

This comparative study has illustrated the strengths and weaknesses of two spectral and a Boussinesq model through comparison with field measurements of coastal wave transformation at three tropical sites. The spectral models STWAVE and SWAN give very similar results and compare reasonably well with measurements prior to wave breaking. Because of the small computational domains and gradual variation of the wave conditions with time, STWAVE provides a reasonable steady-state approximation of the coastal wave field. STWAVE and SWAN show the largest differences in their wave transformations just prior to and during wave breaking due to their different wave breaking mechanisms. COULWAVE is computationally intensive and highly unstable in which small changes in the input conditions can cause the model to fail. Because of this it was difficult to do extensive sensitivity studies with COULWAVE, in particular with the frictional parameters.

Mokuleia gives the clearest comparison of the wave breaking mechanisms employed by the three models. The reef top is fronted by a fairly plain slope offering a more gradual development of the wave breakers in comparison to those occur directly in front of the beach at Waimea and on top of the reef edge at Ipan. The effects of bottom friction appear to be as significant as wave breaking for weaker wave conditions The predictive capabilities of the spectral models appears dependent upon an accurate estimation of the physical roughness, when wave breaking is not the main primary dissipation mechanism. A site specific friction coefficient appears necessary and generally assumed frictional coefficients may not be applicable for predictive purposes. COULWAVE with a typical friction coefficient appears to model the wave energy dissipation.

At Ipan, the spectral models appear to have better predictive capabilities and the results are fairly insensitive to the input friction coefficients. At fringing reefs where wave breaking is the dominant process, it appears that the spectral models breaking mechanisms is sufficient and may be used with more generally assumed frictional parameters to predict nearshore wave transformation. This is also apparent at Mokuleia as the spectral models appear to more properly reduce wave energy during the peak of the swell event with commonly assumed frictional parameters. It is unknown what affects the porous reef face plays in wave energy dissipation and thus it cannot be firmly implied that the spectral models can be accurately used to generally predict wave transformations at sites where breaking is dominant.

It appears that the two important factors that determine the predictive capabilities of the spectral models are the role of bottom friction and the water depth over the reef top. The general predictive capabilities observed from the spectral models appear to be fairly good and can be further improved at Mokuleia with tuning of the frictional parameters. At Ipan the general predictive capabilities appear to be good provided the reef top is not exposed.

Improvements to STWAVE could involve adding the Madsen coefficient to the frictional dissipation mechanisms. This would allow STWAVE to somewhat account for the physical roughness scales in the model itself and would avoid the need to empirically obtain Manning and JONSWAP coefficients for sites where bottom friction is important. An improvement for SWAN could involve the development of a separate breaking criteria fro fringing reef environments. COULWAVE matches the data well at Mokuleia, not as well at Waimea, and does not produce results at Ipan. The inconsistent and sensitive results indicate that COULWAVE might not be suitable for applications with tropical coastal environments.

Table 1. Summary of Swell and Sea events

	Waimea	Mokuleia	Ipan
Start Time	04/19/2006 18:52	03/28/2004 00:29	10/16/2005 00:01
End Time	04/21/2006 16:52	04/09/2004 23:59	10/24/2005 23:31
Duration (hrs)	46	240/72	215.5
Event type	Swell	Seas / Swell	Seas
Average H_s	2.20 m	1.78 /2.40 m	1.51 m
Average T_p	14.8 s	12.6/13.4 s	11.0 s
Average Direction	355°	332°/330°	70°
Max H_s	2.85 m	2.90/4.01 m	2.34 m
T_p at Max H_s	14.3 s	13.3/18.2 s	11.1 s

Table 2. Summary of Waimea Cross-shore Wave Profiles

	Profile 1	Profile 2
Time	04/20/2006 05:52	04/20/2006 15:22
Offshore Hs	1.76 m	2.72 m
Tp	16.67 s	15.38 s
Direction	355°	356°
Tide	0.308 m	0.014 m

Table 3. Summary of Mokuleia Cross-shore Wave Profiles

	Profile 1	Profile 2	Profile 3
Time	04/01/2004 11:59	04/03/2004 07:59	04/0702004 07:59
Offshore *Hs*	1.61 m	2.9 m	4.01 m
Tp	15.38 s	13.33 s	18.18 s
Direction	308°	319°	328°
Tide	0.317 m	-0.039 m	-0.09 m

Table 4. Summary of Guam Cross-shore Wave Profiles

	Profile 1	Profile 2
Time	10/20/2005 05:01	10/22/2005 11:31
Offshore *Hs*	2.28 m	1.41 m
Tp	11.11 s	11.76 s
Direction	67°	71°
Tide	0.213 m	0.277 m

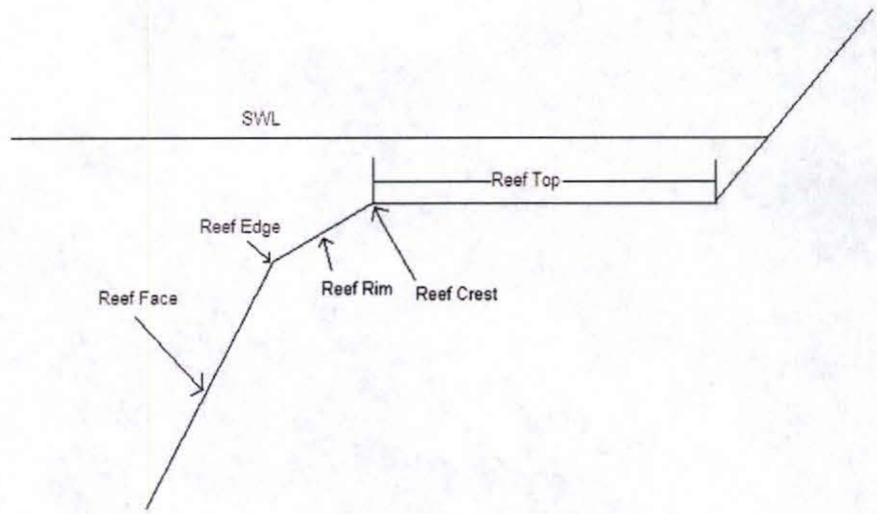

Figure 1. Typical Fringing Reef Morphology

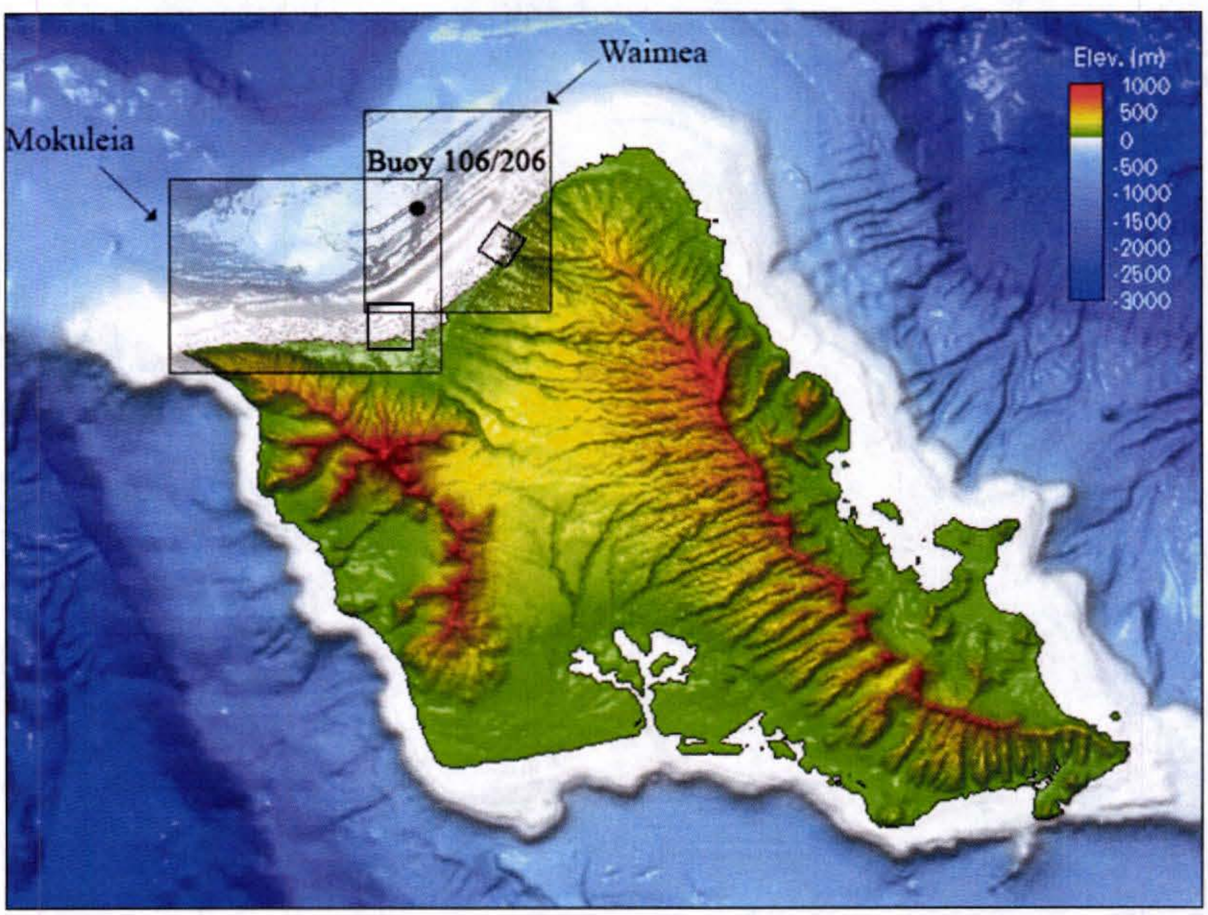

Figure 2. Oahu and Mokuleia and Waimea study sites.

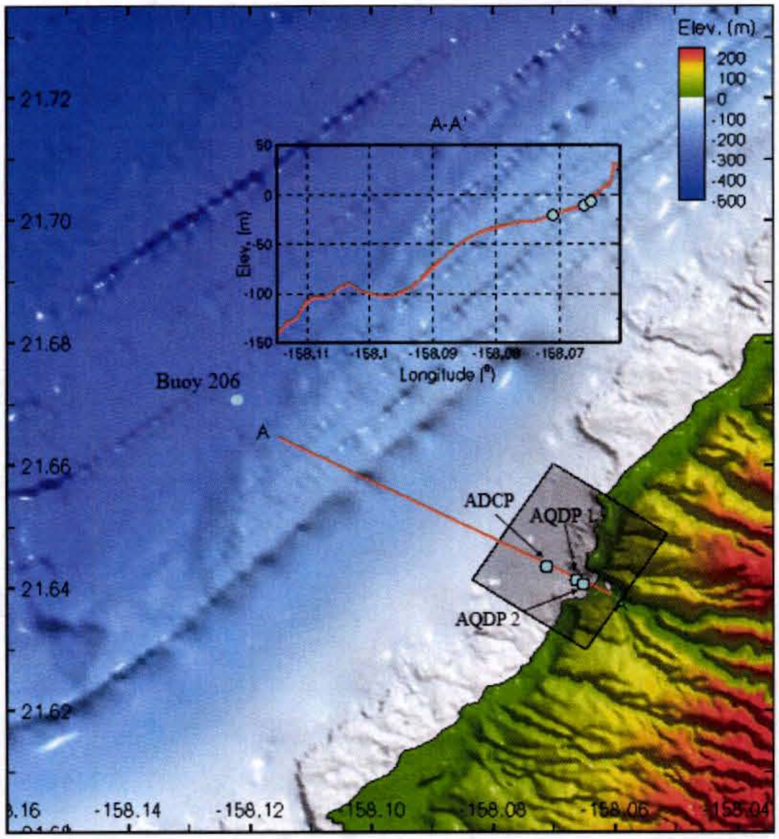

Figure 3. Waimea computational domains and sensor locations

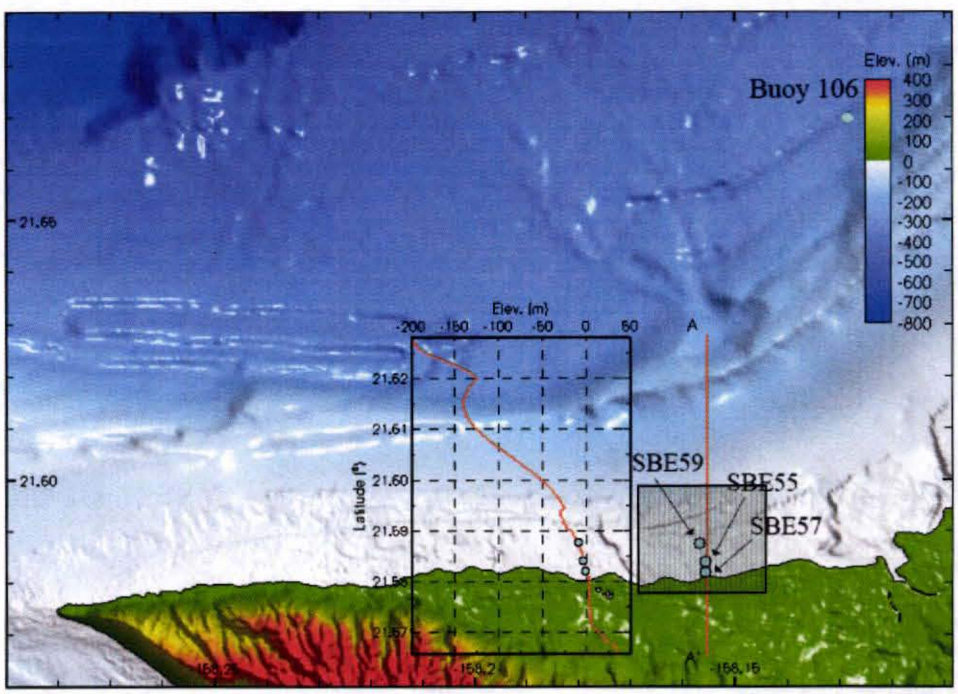

Figure 4. Mokuleia computational domains and sensor locations

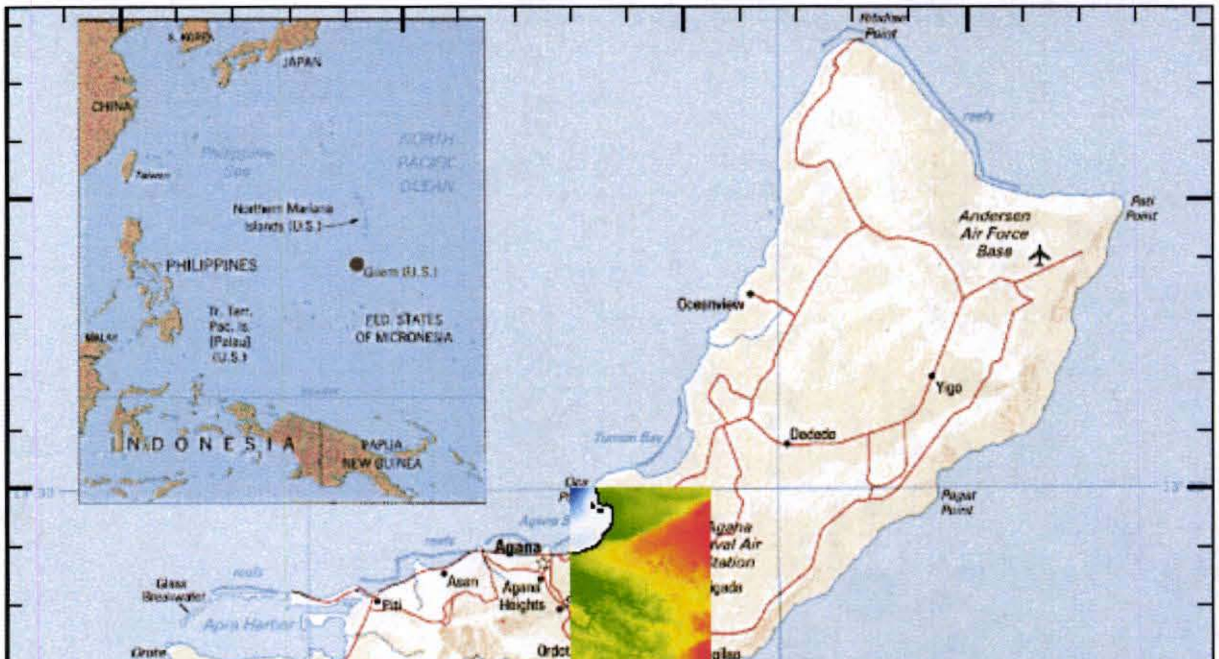

Figure 5. Guam and Ipan study site.

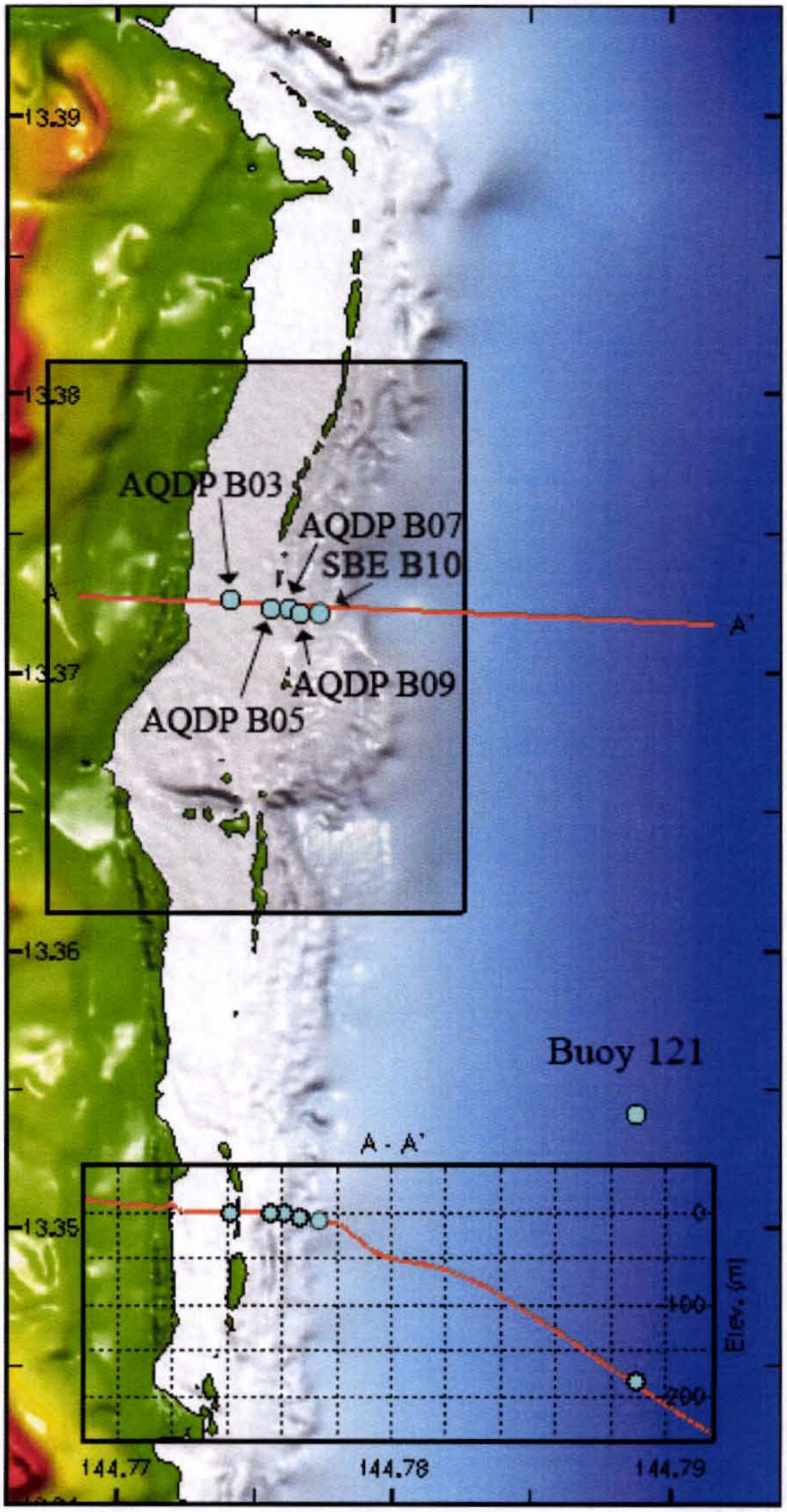

Figure 6. Ipan computational domains and sensor location

(a)

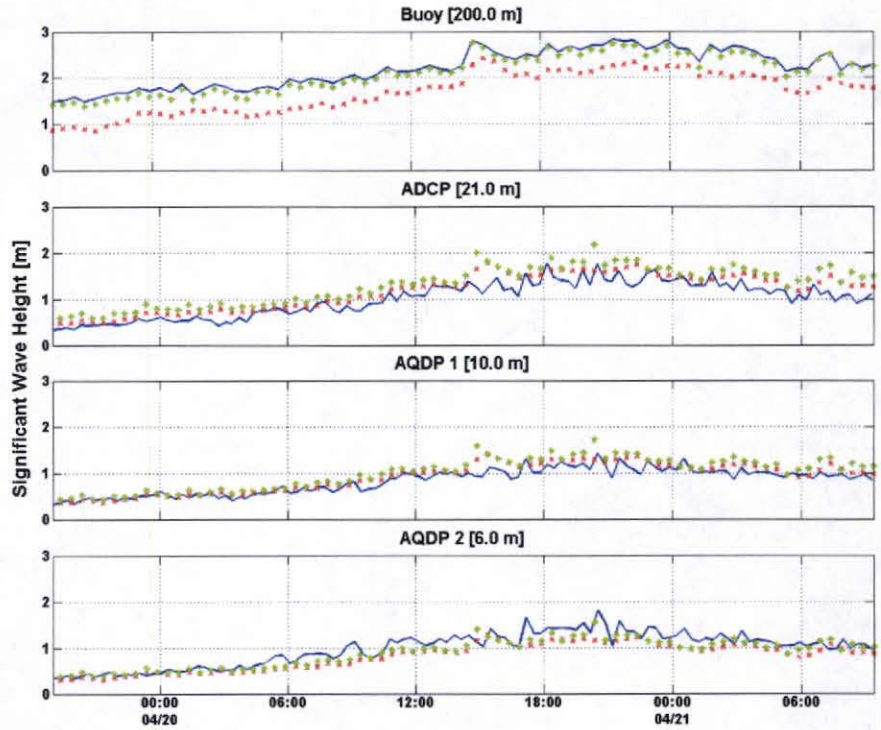

(b)

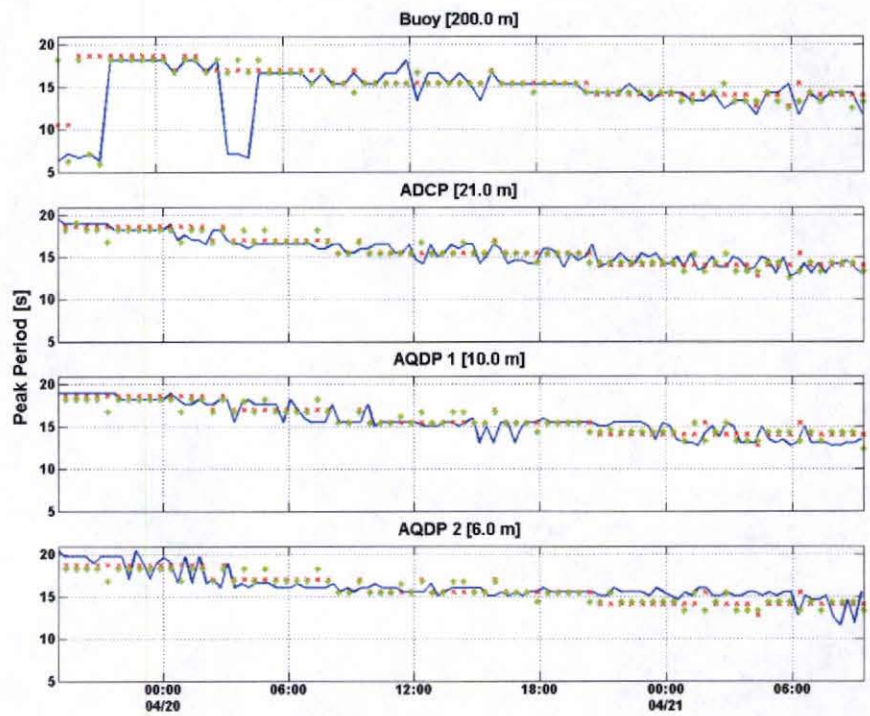

Figure 7. Comparison of (a) significant wave height and (b) peak period at Waimea.
*, STWAVE; *, SWAN; –, sensor measurements

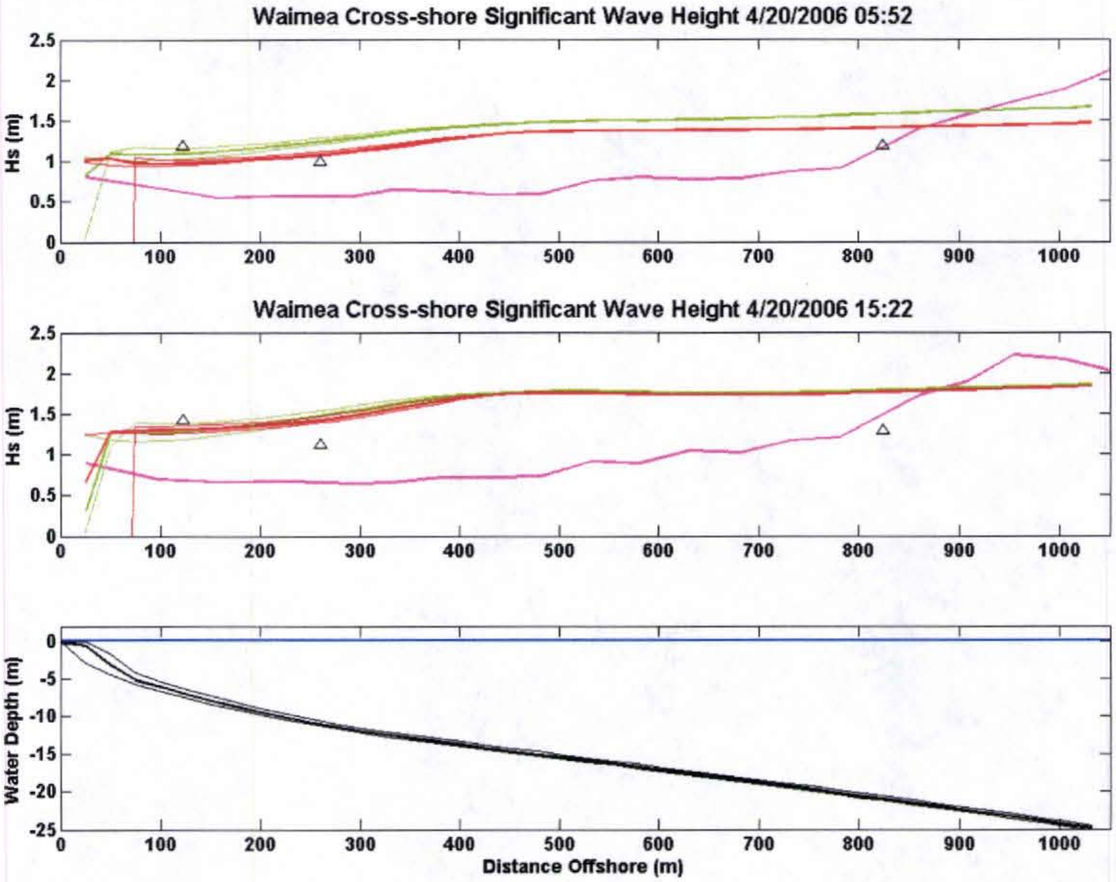

Figure 8. Comparisons of measured and computed significant wave heights along the Waimea nearshore instrument transect. —, STWAVE; —, SWAN; —, COULWAVE; Δ, sensor measurements.

(a)

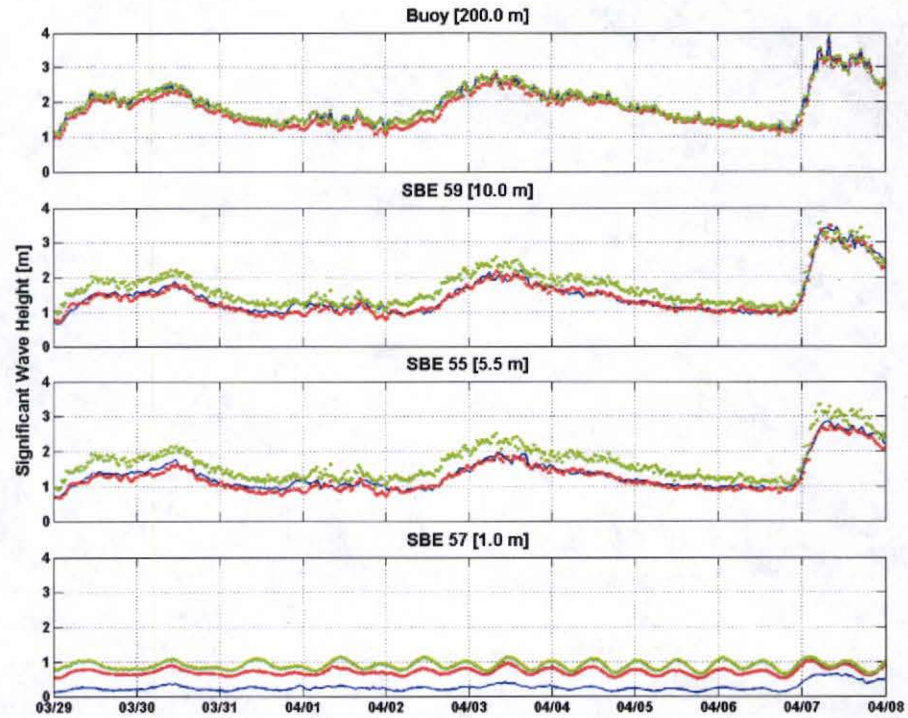

(b)

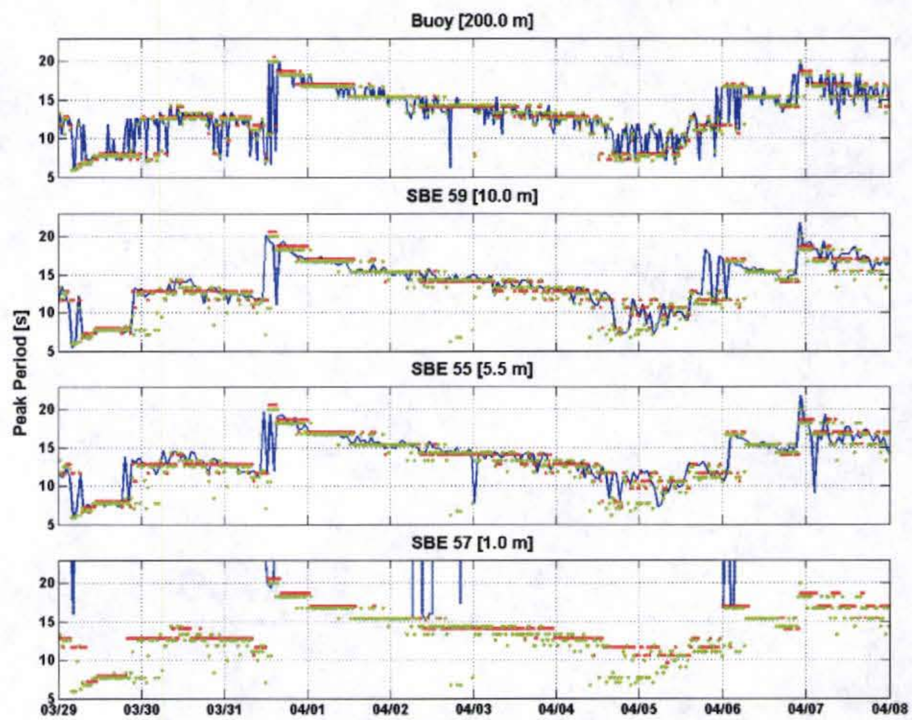

Figure 9. Comparison of (a) significant wave height and (b) peak period at Mokuleia.
*, STWAVE; *, SWAN; –, sensor measurements.

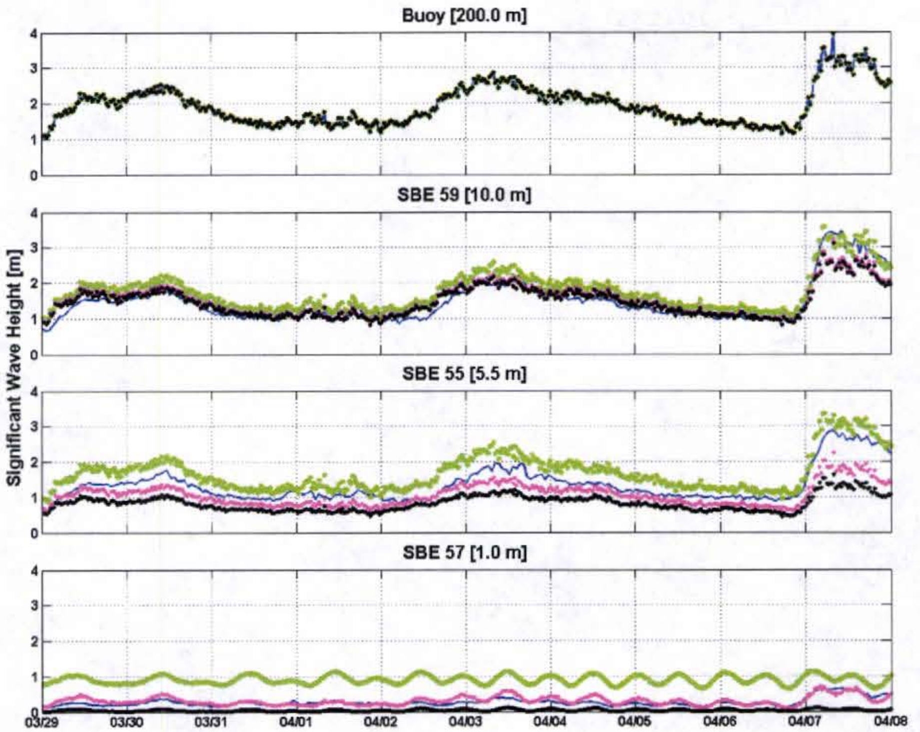

Figure 10. Comparison of significant wave height for varying bottom friction coefficients in STWAVE. *, n = 0.035; *, n = 0.2; *, $c_f = 0.12$; —, sensor measurements.

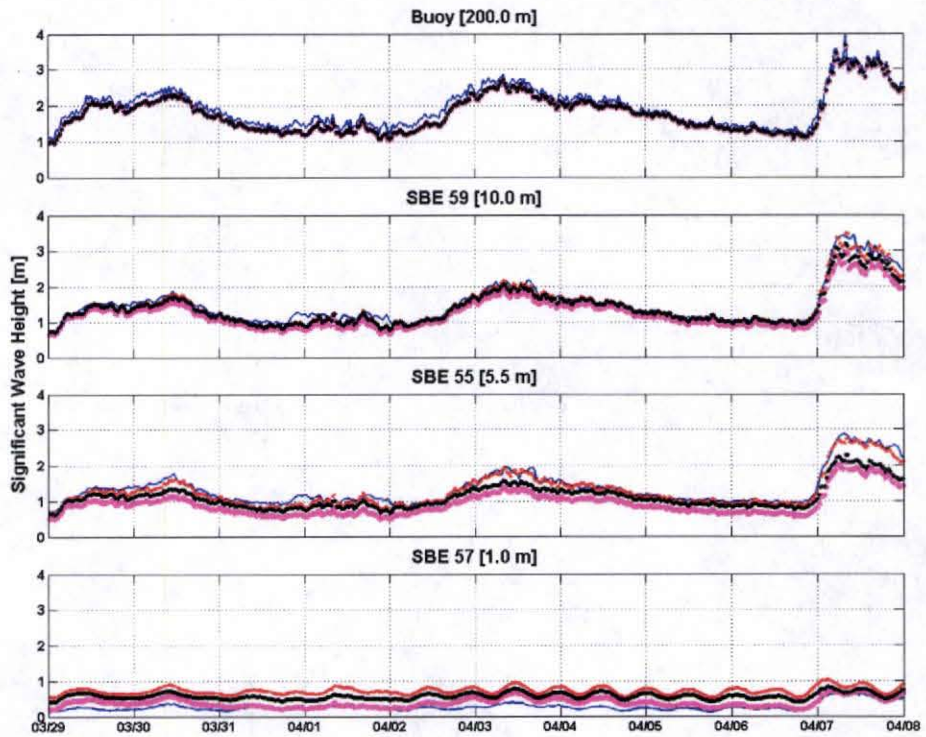

Figure 11. Comparison of significant wave height for varying bottom friction coefficients in SWAN. *, $K_N = 0.2$; *, $K_N = 1.0$; *, $c_{JON} = 1.14$; —, sensor measurements.

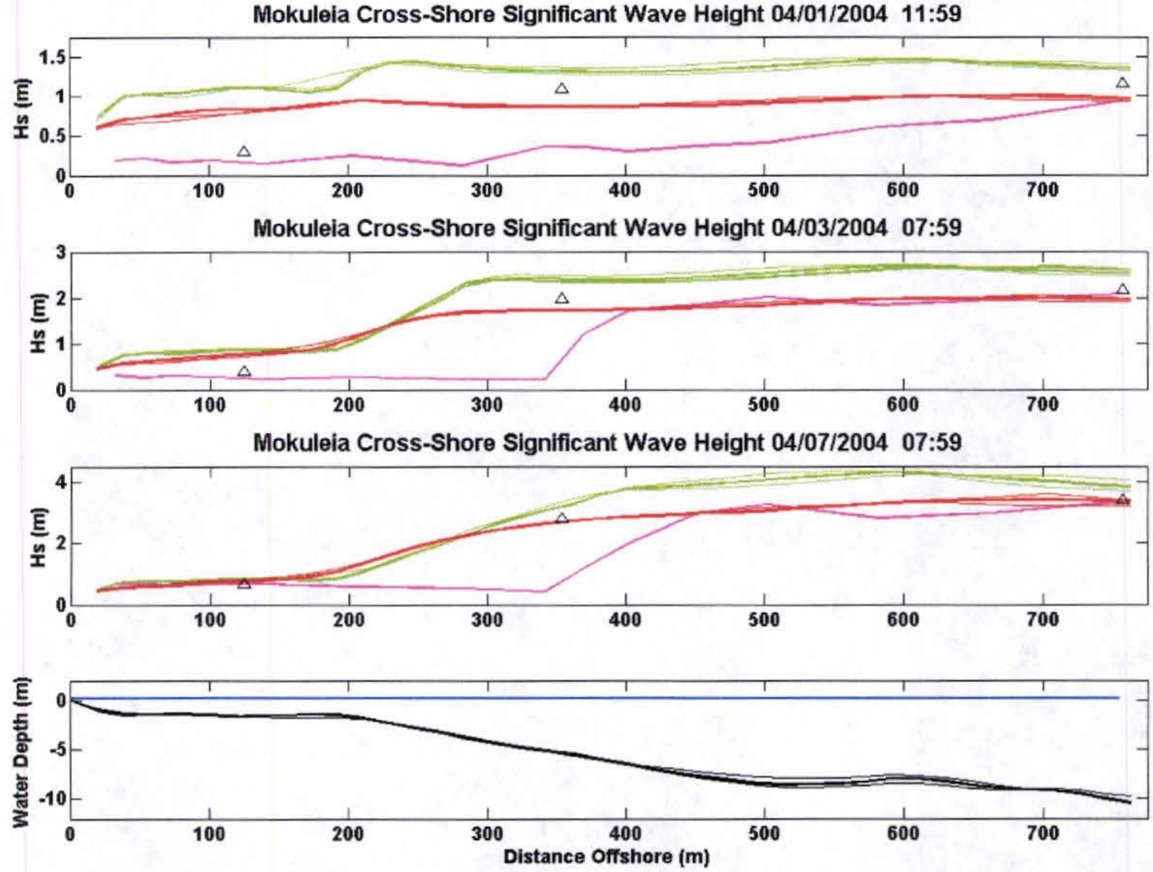

Figure 12. Comparisons of measured and computed significant wave heights along the Mokuleia nearshore instrument transect. —, STWAVE; —, SWAN; —, COULWAVE; Δ, sensor measurements.

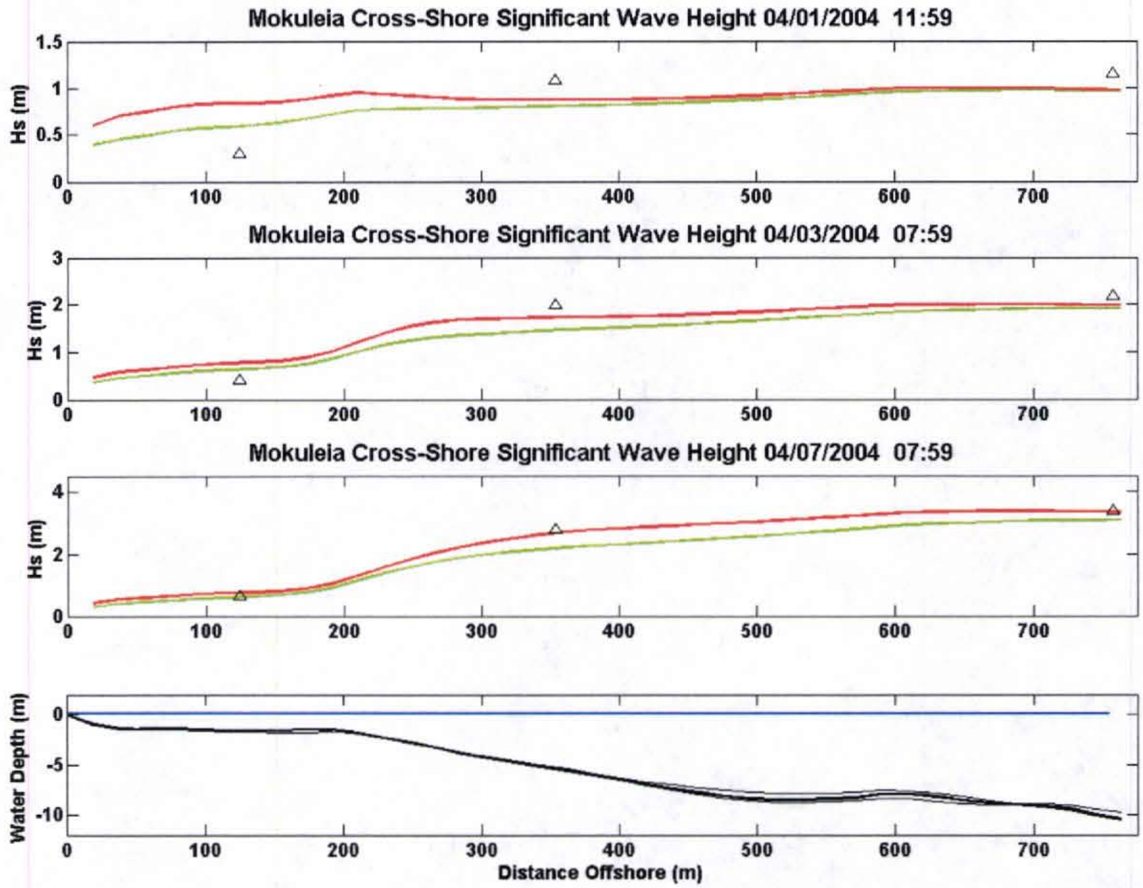

Figure 13. Comparisons of measured K_N values for SWAN along the Mokuleia nearshore instrument transect. —, $K_N = 0.2$; —, $K_N = 1.0$; Δ, sensor measurements.

(a)

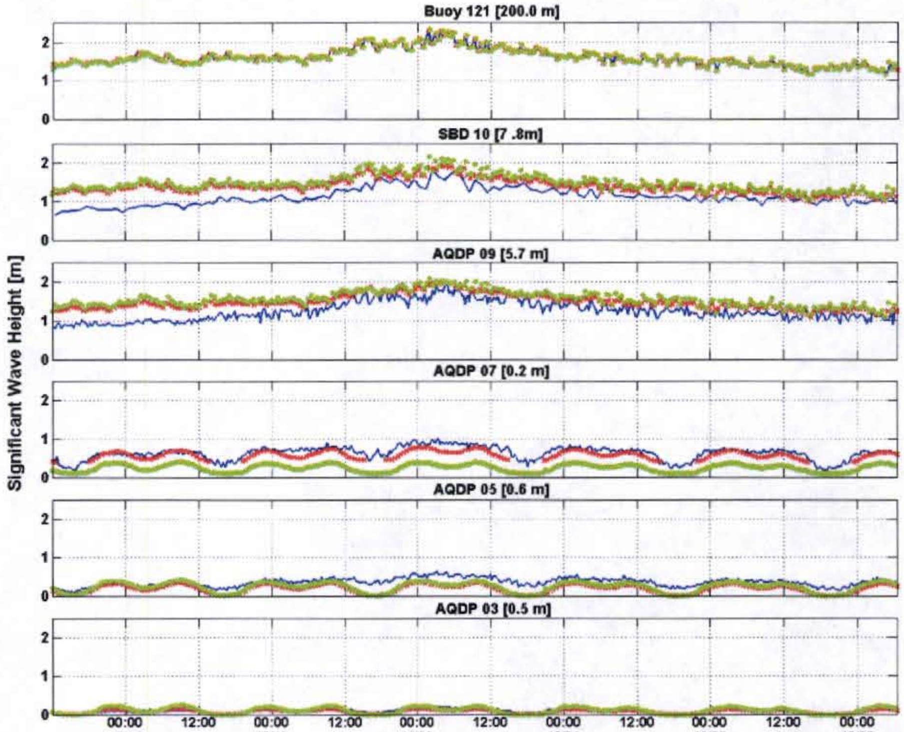

(b)

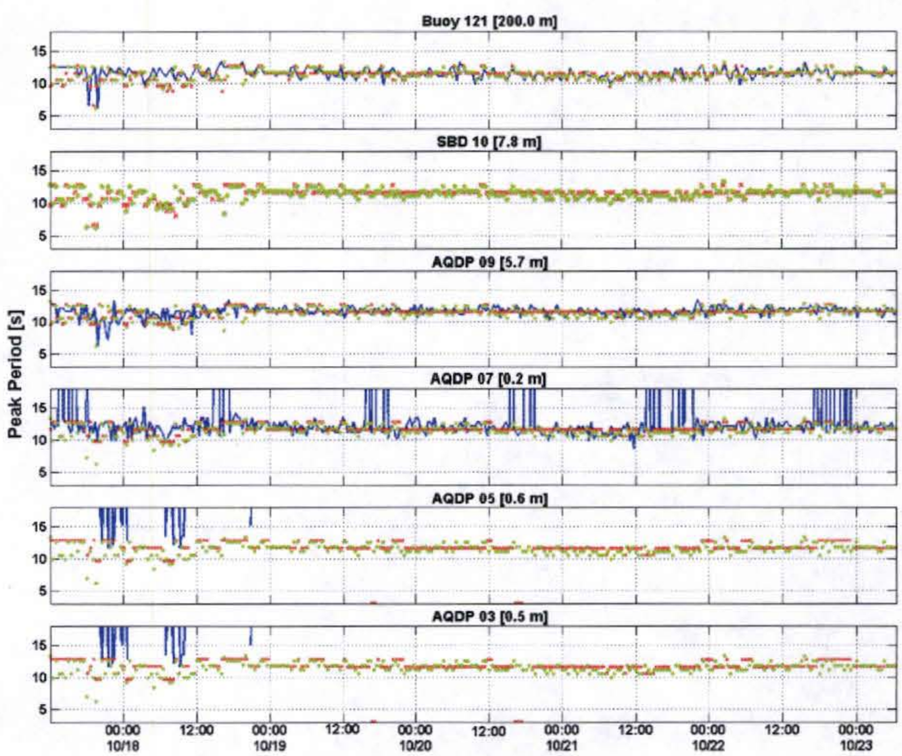

Figure 14. Comparison of (a) significant wave height and (b) peak period at Ipan.
*, STWAVE; *, SWAN; –, sensor measurements.

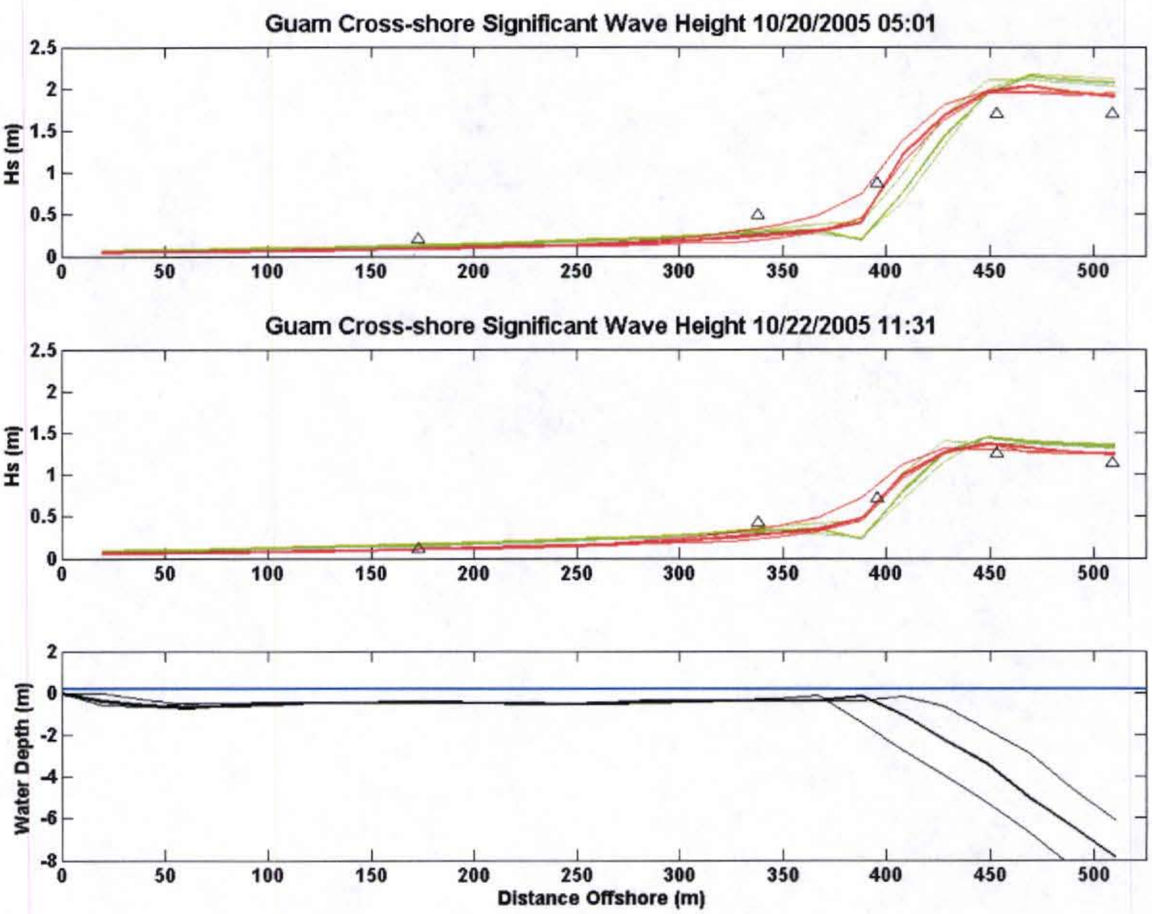

Figure 15. Comparisons of measured and computed significant wave heights along Ipan nearshore instrument transect. —, STWAVE; —, SWAN; Δ, sensor measurements.

References

Black, K.P. (1978). Wave Transformation over a Shallow Reef. Look Laboratory. Technical Report No.42, University of Hawaii Sea Grant College Program, Honolulu, Hawaii.

Booji, N.C., Ris, R.C., and Holthuijsen, L.H. (1999). "A third-generation wave model for coastal regions, Part I, Model description and validation." *Journal of Geophysical Research*, 104(C4), 7649-7666.

Delft University of Technology. (2006). SWAN User Manual, SWAN Cycle III version 40.51

Gerritsen, F. (1981). Wave Attenuation and Setup on a Coastal Reef. Look Laboratory Technical Report No.48, University of Hawaii Sea Grant College Program, Honolulu, Hawaii.

Hardy, T.A. and Young, I. (1996). "Field study of wave attenuation on an offshore coral reef." *Journal of Geophysical Research*, 101(C6), 14311-14326.

Hasselman, K., et al. (1973). "Measurements of wind-wave growth and swell decay during the Joint North Sea Wave Project (JONSWAP." *Dtsch. Hydrogr. Z. Suppl.*, 12(A8), 1-95.

Lowe, R.J., et al. (2005). "Spectral wave dissipation over a barrier reef." *Journal of Geophysical Research*, 110, C04001, doi:10.1029/2004JC002711.

Lugo-Fernandez A., Roberts, H.H., and Suhayda, J.N. (1998). "Wave transformations across a Caribbean fringing-barrier coral reef." *Continental Shelf Research*, 18, 1099-1124.

Lynett, P.J., Wu, T.-R., and Liu, P.L.-F. (2002). "Modeling wave runup with depth-integrated equations". *Coastal Engineering*, 46(2), 89-108.

Madsen, O.S., Y.-K. Poon and H.C. Graber, (1988). Spectral wave attenuation by bottom friction: Theory, Proc. 21th Int. Conf. Coastal Engineering, ASCE, 492-504

Mortensen, S. (2006). Numerical Modeling of the Surf Zone Dynamics in Waimea Bay. MS Thesis, Technical University of Denmark, Lyngby, Copenhagen.

Nwogu, O., 1993. "Alternative form of Boussinesq equations for nearshore wave propagation." *Journal of Waterway, Port, Coastal, and Ocean Engineering*, 119(6), 618–638.

Resio, D.T. (1987). "Shallow-water waves. I: Theory." *Journal of Waterway, Port, Coastal, and Ocean Engineering*, 113(3), 264–281.

Resio, D.T. (1988). "Shallow-water waves. II: Data comparisons." *Journal of Waterway, Port, Coastal, and Ocean Engineering*, 114(1), 50-65.

Ris, R.C., Holthuijsen, H., and Booji, N. (1999). "A third-generation wave model for coastal regions, Part II, Verification." *Journal of Geophysical Research*, 104(C4), 7667-7681.

Smith, J.M., and Resio, D.T., (2004). "Improved shallow-water wave modeling." *Proceedings, 8th International Workshop on Wave Hindcasting and Forecasting*, Environment Canada, North Shore, Oahu, N1.

Smith, J.M., Sherlock, A.R., and Resio, D.T. (2001). STWAVE: steady-state spectral wave model; user's manual for STWAVE Version 3.0. Instruction Report, U.S. Army Engineer Research and Development Center, Vicksburg, MS.

Vetter, O.J. (2006). Field Observations of Setup Over Two Fringing Reefs: Ipan Reef, Guam and Mokule'ia Reef, Hawai'i. MS Thesis, University of Hawaii, Honolulu, Hawaii.

Wei, Y., Mao, X.Z., and Cheung, K.F. (2006). "Well-balanced finite volume model for long-wave runup". *Journal of Waterway, Port, Coastal, and Ocean Engineering*, 132(2), 114-124.

Winder, B.J. (1996). The Theory, Documentation, and Verification of a Steady-State Spectral Wave Model: STWAVE. MS Thesis, Florida Institute of Technology, Melbourne, Florida.

Wu, Y.Y. and Cheung, K.F. (2007). "Explicit solution to the Riemann problem for nonlinear shallow-water equations." *International Journal for Numerical Methods in Fluids*, Doi: 10.1002/FLD1696.

Young, I.R. (1989). "Wave transformation over coral reefs." *Journal of Geophysical Research*, 94(C7), 9770-9789.